

Ground-state properties of the Rokhsar–Kivelson dimer model on the triangular lattice

A. Ioselevich,¹ D. A. Ivanov,² and M. V. Feigelman¹

¹*Landau Institute for Theoretical Physics, 117940 Moscow, Russia*

²*Theoretische Physik, ETH-Hönggerberg, CH-8093 Zürich, Switzerland*

(Dated: June 21, 2002)

We explicitly show that the Rokhsar–Kivelson dimer model on the triangular lattice is a liquid with topological order. Using the Pfaffian technique, we prove that the difference in local properties between the two topologically degenerate ground states on the cylinders and on the tori decreases exponentially with the system size. We compute the relevant correlation length and show that it equals the correlation length of the vison operator.

I. RVB LIQUID AND THE ROKHSAR–KIVELSON DIMER MODEL

Resonating valence bond (RVB) spin liquid in two dimensions is a remarkable theoretical concept which predicts very unusual low-temperature properties of spin-1/2 systems[1]. Unlike conventional magnetically-ordered ground states with spin-1 excitations, the RVB ground state has no long-range order of any local order parameter and possesses elementary excitations with spin 1/2[2]. If such a system is doped with mobile holes, the fractionalization of spin excitations translates into the effect of spin-charge separation: this scenario has been widely explored in the context of high-temperature superconductivity[2, 3, 4]. While a rigorous verification of the RVB liquid phase in a realistic spin system is usually very difficult due to the strongly-correlated nature of the state, many specially designed systems have confirmed RVB liquid properties[5, 6, 7, 8, 9, 10].

In understanding generic properties of the RVB liquid state, one may benefit from studying dimer models which are closely related to the RVB spin liquids[11, 12]. In the RVB construction, the wave function is represented as a sum over singlet configurations, while in the dimer models the singlets are replaced by dimers. The difference between the spin and the dimer systems is that dimer configurations are mutually orthogonal by definition, while different singlet configurations have a finite overlap[13]. The RVB spin liquid is known to have two types of elementary excitations: spinons (spin-1/2 excitations) and visons (Z_2 vortices) [4, 14]. In a dimer liquid, the spinons are prohibited by the dimer constraint (or, equivalently, are pushed infinitely high in energy), while the visons are expected to be indeed the lowest excitations above the ground state. The RVB spin liquid must have topological degeneracy on domains of nontrivial topology. Such a decoupling into topological sectors is straightforward in dimer liquids where it is defined in purely geometric terms[14, 15, 16]. Thus dimer models provide a convenient test ground for studying properties of RVB liquids related to vison excitations.

The advantage of studying dimer models is that they are simpler than spin models, and are hence better understood and more accessible to analytical methods. The

simplest dimer model contains the pair-wise hopping term and the pair-wise potential term

$$H = \sum_{\square} [-t(|\boxminus\rangle\langle\boxplus| + |\boxplus\rangle\langle\boxminus|) + v(|\boxminus\rangle\langle\boxminus| + |\boxplus\rangle\langle\boxplus|)] , \quad (1)$$

where the sum is taken over the four-vertex plaquets of the lattice[15]. On the square lattice such a model has a crystal ground state (with the crystal of dimers breaking the translational symmetry of the lattice) for any ratio v/t , except for the phase-transition point(s) between different crystal structures[11, 15, 17]. The situation is different on the triangular lattice (with the sum in (1) taken over all rhombi consisting of two neighboring triangles): there the dimers are believed to form a liquid in a finite range of the parameter v/t [6, 18]. Out of all possible values of v/t , one is special: $v/t = 1$. At this ratio of parameters — further called Rokhsar–Kivelson (RK) point — the ground state of the Hamiltonian (1) is known exactly: it is a superposition of all possible dimer configurations with equal amplitudes [unfortunately, the excited states are not known exactly even at the RK point]. At $v/t > 1$, this state immediately yields to the staggered crystal state via a first-order phase transition. However at $v/t < 1$, from the available numerical evidence it follows that the RK state on the triangular lattice smoothly evolves without crystallization in a finite range of v/t (approximately until $v/t \approx 0.6 \dots 0.8$)[6, 18]. It is this region of the parameter space which contains the dimer liquid.

The RK point is one of the representatives of the liquid phase and is most accessible for analytic treatment, because averaging over the ground state is equivalent to the statistical averaging over all possible dimer configurations. Such an averaging may be performed with the usual Pfaffian technique[19] which allows to establish the exponential decay of dimer correlations[6]. In this paper, we employ the Pfaffian technique to explicitly compute the correlation length involved in the ground-state correlation functions and in the splitting between the topological sectors on the cylinder and on the torus. We further demonstrate that the same correlation length also appears in the vison correlation function. Thus our calculations prove that the RK ground state on the triangular lattice possesses topological order: on a topologically

nontrivial domain, the ground states in different topological sectors are degenerate and locally indistinguishable (in the limit of infinite system size). Note that the exponential decay of ground-state correlation functions is consistent with the numerical finding of the gap in the excitation spectrum at the RK point (the magnitude of the gap is numerically estimated as $0.1t$) [18, 20].

II. PFAFFIAN TECHNIQUE AND CORRELATION LENGTHS

In the Pfaffian technique, the statistical averaging over the dimer configurations is performed via introducing an auxiliary real fermionic variable (a Majorana fermion) on each lattice site [19]. The total number of dimer configurations may then be written as the partition function of these fermions

$$Z = \int \prod_i da_i \exp \left[\sum_{ij} a_i A_{ij} a_j \right] = \text{Pfaff}(A_{ij}), \quad (2)$$

where i and j label the lattice sites, and the fermionic variables a_i obey the conventional rules: $a_i a_j = -a_j a_i$, $\int da_i = 0$, $\int a_i da_i = 1$. The “hopping amplitudes” A_{ij} take values ± 1 on nearest-neighbor sites and 0 otherwise, and form an antisymmetric matrix: $A_{ij} = -A_{ji}$. The signs of A_{ij} must be adjusted so that all terms in the expansion of the exponent in (2) give positive weight. Such terms in the expansion of the exponent are in one-to-one correspondence to the dimer coverings of the lattice. Each of them has magnitude one, and should they all have equal signs, the partition function (2) simply counts the total number of dimer coverings.

As shown in Ref. 19, a necessary requirement for the proper relative sign of different dimer coverings is that the circular product $\prod A_{ij}$ equals (-1) around any elementary rhombus (around any elementary even-length

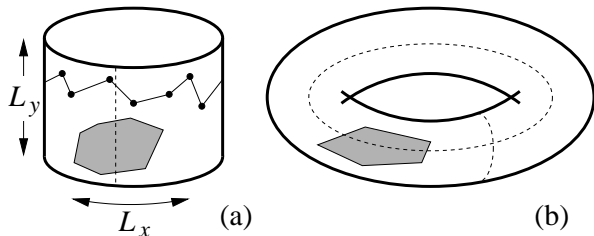


FIG. 1: Topological sectors on a cylinder and on a torus. Dimer coverings may be classified according to the parities of the number of dimers intersecting the reference lines (dashed lines). Dimer configurations differing by a rearrangement in contractible domains (shaded areas) belong to the same topological sector and contribute with the same sign to the partition function (2). To change the topological sector, a circular permutation of dimers along a topologically nontrivial contour (shown in a zig-zag line in the case of the cylinder) is necessary.

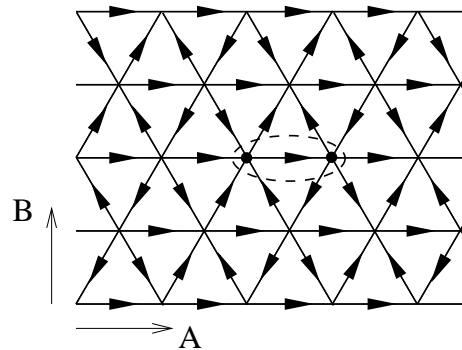


FIG. 2: One possible choice of the amplitudes A_{ij} . This choice of amplitudes is periodic with a unit cell containing two lattice sites (marked by a dashed ellipse). The arrow directions correspond to the signs of A_{ij} : A_{ij} equals 1 if the arrow points from i to j , and equals -1 if it points from j to i . Also shown are A and B directions: parallel and perpendicular to the lattice lines, respectively.

cycle, in the general case of a planar lattice). Then it follows that $\prod A_{ij} = -1$ over any *contractible* contour of even length and, as a consequence, any two dimer configurations differing by a *local* rearrangement of dimers contribute to the partition function (2) with equal signs. Different dimer configurations which cannot be related by local dimer rearrangements (i.e. by rearrangements in a contractible domain, see Fig. 1) may contribute with either equal or opposite signs: this effect will be of crucial importance for our calculation.

One possible choice of the amplitudes A_{ij} is shown in Fig. 2. Note that in order to obey the sign rule for A_{ij} we have to double the unit cell of the lattice. However, any physical quantity computed with those A_{ij} has the periodicity of the lattice, as the set of amplitudes A_{ij} translated by one lattice spacing may be returned to the original form by an appropriate Z_2 gauge transformation $A_{ij} \mapsto W_i A_{ij} W_j$ with $W_i = \pm 1$. Now the partition function (2) as well as correlation functions may be conveniently computed in the Fourier components. The Fourier transformation of A_{ij} is a 2×2 matrix $A(\mathbf{k})$. From antisymmetry of the matrix A_{ij} it follows that its eigenvalues always come in pairs $\pm iE(\mathbf{k})$, with complex conjugate eigenvectors corresponding to opposite eigenvalues. A straightforward calculation shows that, for the triangular lattice, the spectrum of $A(\mathbf{k})$ in the bulk is always gapped (never crosses zero as a function of \mathbf{k}). Explicitly, it is given by

$$E(\mathbf{k}) = 2 (\cos^2 k_1 + \cos^2 k_2 + \cos^2 k_3)^{1/2}, \quad (3)$$

where k_1 , k_2 , and k_3 are the projections of the vector \mathbf{k} onto the three lattice directions (obeying the constraint $k_1 + k_2 + k_3 = 0$). We have also shifted the origin of the Brillouin zone to bring (3) to a symmetric form. The gap in the spectrum of A_{ij} is crucial for the exponential decay of correlation functions: as we shall see below, the correlation length is determined by the complex wave

vectors \mathbf{k} solving the equation $E(\mathbf{k}) = 0$ [6]. At this stage of calculation, we see the difference between the triangular and square lattices: on the square lattice, the corresponding matrix A_{ij} leads to a gapless spectrum (and, consequently, to the power-law decay of correlations[21]. Note that although the presence or absence of the gap in the matrix A_{ij} (governing the decay of correlation functions in the ground state) agrees with the presence or absence of the gap for excitations, there is no direct relation between the two gaps. The spectrum of A_{ij} is not the energy spectrum of quantum dimers, but only the spectrum of auxiliary Majorana fermions introduced for calculating the classical partition function of all dimer configurations.

Correlation functions of dimers may be expressed in terms of Green's functions of Majorana fermions. Indeed, the probability of dimers occupying a given set of positions (connecting pairwise points 1 and 2, 3 and 4, \dots , $2m-1$ and $2m$) may be computed by excluding those points from the lattice, which is equivalent to placing Majorana fermions at those points:

$$\begin{aligned} \langle n_{12} \dots n_{2m-1, 2m} \rangle &= \langle a_1 a_2 \dots a_{2m} \rangle \\ &\equiv Z^{-1} \int \prod_i da_i (a_1 a_2 \dots a_{2m}) \exp \left[\sum_{ij} a_i A_{ij} a_j \right] \end{aligned} \quad (4)$$

(up to a sign). Here the first average denotes the statistical averaging of dimer occupation numbers n_{ij} over all dimer configurations, while the second average is the quantum-mechanical correlation function in the theory of Majorana fermions. This correlation function may further be decoupled using the Wick theorem.

The Green's functions are obtained as

$$G(i, j) \equiv \langle a_i a_j \rangle = \int_{\text{B.Z.}} d\mathbf{k} A^{-1}(\mathbf{k}) e^{i\mathbf{k}(\mathbf{r}_i - \mathbf{r}_j)}, \quad (5)$$

with the integral over \mathbf{k} defined as averaging over the Brillouin zone. The decay at large distances is found from deforming the integration domain into complex values until it reaches the singularities in $A^{-1}(\mathbf{k})$. The singularities are the square-root branching points, which translates into the asymptotics $G(R) \propto R^{-1/2} \exp(-R/\xi)$. The correlation length ξ is direction-dependent. In the direction specified by a unit vector \mathbf{n} , the correlation length $\xi_{\mathbf{n}}$ is given by $\xi_{\mathbf{n}}^{-1} = -i\mathbf{k}_{\mathbf{n}}\mathbf{n}$, where the complex vector $\mathbf{k}_{\mathbf{n}}$ is determined from the set of equations:

$$E(\mathbf{k}_{\mathbf{n}}) = 0; \quad (6)$$

$$\nabla E(\mathbf{k}_{\mathbf{n}}) \parallel \mathbf{n}. \quad (7)$$

(the meaning of the second equation is that the “group velocity” is directed along the vector \mathbf{n}). Equivalently, the conditions (6), (7) for $\mathbf{k}_{\mathbf{n}}$ may be expressed as

$$\xi_{\mathbf{n}}^{-1} = \max \min^{\text{Re}} (-i\mathbf{k}\mathbf{n}) \big|_{E(\mathbf{k})=0}, \quad (8)$$

where $\max \min^{\text{Re}}$ denotes minimizing the real part (among its positive values) over the components of \mathbf{k}

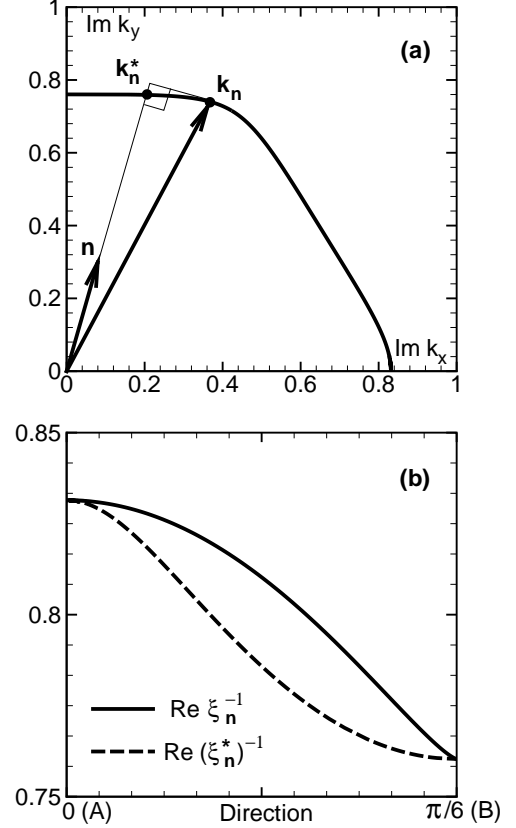


FIG. 3: Correlation length and its direction dependence. (a) Construction of the correlation length. In the $(\text{Im } k_x, \text{Im } k_y)$ plane, there is a region around $\text{Im } \mathbf{k} = 0$ where there are no solutions to the equation $E(\mathbf{k}) = 0$. The thick solid line denotes the boundary of this region [the axis k_x is chosen along one of the lattice directions (A direction), and the axis k_y is perpendicular to it (B direction); if reflected in those two axes, the thick solid line has the hexagonal symmetry]. Given the direction \mathbf{n} , the vector $\text{Im } \mathbf{k}_{\mathbf{n}}$ is chosen on this boundary to maximize its projection onto \mathbf{n} [in accordance with (6), (7), or, equivalently, with (8)] The vector $\mathbf{k}_{\mathbf{n}}$ determines the correlation length $\xi_{\mathbf{n}}^{-1} = -i\mathbf{n}\mathbf{k}_{\mathbf{n}}$ in the \mathbf{n} direction. For a vison tunneling as a wave front [Eq. (16)], the tunneling amplitude has a different correlation length given by $(\xi_{\mathbf{n}}^*)^{-1} = -i\mathbf{n}\mathbf{k}_{\mathbf{n}}^*$ with the imaginary component of the vector $\mathbf{k}_{\mathbf{n}}^*$ parallel to \mathbf{n} . (b) The direction dependence of the real parts of the inverse correlation lengths $\xi_{\mathbf{n}}^{-1}$ and $(\xi_{\mathbf{n}}^*)^{-1}$. The inverse correlation lengths are plotted versus the angle between the direction \mathbf{n} and the lattice lines. The angle 0 corresponds to the A direction, and the angle $\pi/6$ corresponds to the B direction.

parallel to \mathbf{n} and maximizing it over the perpendicular components. The vectors \mathbf{k} are confined to the complex surface $E(\mathbf{k}) = 0$. The construction of $\xi_{\mathbf{n}}^{-1}$ is illustrated in Fig. 3.

In the particular cases of directions A and B parallel and perpendicular to the lattice lines respectively (as shown in Fig. 2), the correlation lengths may be found

analytically (from solving (6) and (7))

$$\xi_A^{-1} = \frac{1}{2} \ln \left(1 + \sqrt{3} + \sqrt{2\sqrt{3} + 3} \right) \pm i \arctan \sqrt{\frac{2}{\sqrt{3}}} - 1$$

$$\approx 0.83 \pm 0.12 i\pi, \quad (9)$$

$$\xi_B^{-1} = \frac{1}{\sqrt{3}} \ln \left(2 + \sqrt{3} \right) \approx 0.76 \quad (10)$$

(in the units of the lattice constant). The imaginary part in ξ_A^{-1} implies the damped oscillating asymptotic behavior (with an incommensurate wave vector) of the Green's function and of other relevant correlations (e.g., vison correlation function, see Section V).

For other directions, the equations (6) and (7) [or, equivalently, (8)] may be solved numerically. In Fig. 3, we plot the direction dependence of the inverse coherence length ξ_n^{-1} .

The exponential decay of the Green's functions implies an exponential decay of all dimer-dimer correlations. For example, the pair-wise dimer correlation $\langle n_{12} n_{34} \rangle$ decays with the correlation length $\xi/2$, since it involves a product of two Green's functions[6].

III. TOPOLOGICAL DEGENERACY ON MULTIPLY-CONNECTED DOMAINS

If one considers dimer coverings on a domain of non-trivial topology (e.g., torus, cylinder, domains with holes, etc.), such coverings may be classified into topological classes[14, 16]. Dimer coverings from different topological classes cannot be transformed into each other by local rearrangements of dimers. The topological classes are defined by the parity of the number of dimers intersecting a given non-contractible closed contour. On the cylinder there are two topological classes, on the torus there are four of them (Fig. 1).

In the quantum dimer model, the Hilbert spaces spanned by different topological classes are not mixed by the Hamiltonian, and each topological class possesses its own ground state. At the RK point, each of these ground states has zero energy. In the general case of a topological liquid, the splitting of energies between different topological sectors must be exponentially suppressed in system size[4, 11]. We verify this property later near the RK point to the lowest-order perturbation theory in $(v/t - 1)$.

At the RK point, we compare correlation functions in different topological sectors. We shall see that the correlators in different sectors nearly coincide, with the splitting exponentially small in system size. We start our analysis with comparing partition functions for different topological sectors. The derivation looks different for the cases of the torus and of the cylinder.

Consider first the topological sectors on the torus. Denote the numbers of dimer coverings with even/odd intersection indices at reference contours by N_{ee} , N_{eo} , N_{oe} ,

and N_{oo} , where $N_{\epsilon_x \epsilon_y}$ corresponds to the sector with the parity ϵ_x of intersection with the line parallel to y -axis, and the parity ϵ_y is of intersection with the line parallel to x -axis. In the Pfaffian technique, different topological sectors may be accessed by imposing either periodic or antiperiodic boundary conditions across the reference contours (in the x and y directions)[14, 16, 22]. The corresponding partition functions $Z_{\sigma_x \sigma_y}$ ($\sigma_x, \sigma_y = \pm$) are expressed in terms of $N_{\epsilon_x \epsilon_y}$ as

$$\begin{aligned} Z_{++} &= N_{ee} + N_{eo} + N_{oe} - N_{oo}; \\ Z_{+-} &= N_{ee} - N_{eo} + N_{oe} + N_{oo}; \\ Z_{-+} &= N_{ee} + N_{eo} - N_{oe} + N_{oo}; \\ Z_{--} &= -N_{ee} + N_{eo} + N_{oe} + N_{oo}. \end{aligned} \quad (11)$$

(up to the simultaneous change of signs of σ_x and/or σ_y in all the four expressions above: the particular choice of signs of σ_x and σ_y depends on the gauge choice for A_{ij} ; the overall sign of $Z_{\sigma_x \sigma_y}$ is ignored, as usual). These expressions are a particular case of a more general formula for surfaces of arbitrary genus[23]. We now establish that the splitting in $Z_{\sigma_x \sigma_y}$ is exponentially small in the system size, then the same exponential smallness will follow for the splitting of $N_{\epsilon_x \epsilon_y}$. Consider, for example, the partition functions Z_{++} and Z_{+-} . Each of them is given by the sum over the Brillouin zone

$$Z_{\sigma_1 \sigma_2} = \exp \sum_{\text{B.Z.}} \ln E(\mathbf{k}), \quad (12)$$

where the lattice of points \mathbf{k} is determined by the boundary conditions. In the partition functions Z_{++} and Z_{+-} , the lattices of \mathbf{k} are shifted by half a period in the y -direction. We can rewrite the relative difference Δ in those partition functions as a sum over trajectories with odd windings in the y -direction (taking the Fourier transform of $\ln E(\mathbf{k})$ and using the Poisson summation formula):

$$\begin{aligned} \Delta &= \frac{Z_{++} - Z_{+-}}{Z} = \sum_{\text{B.Z.}} \ln E(\mathbf{k}) - \sum'_{\text{B.Z.}} \ln E(\mathbf{k}') \\ &= \sum_{\mathbf{R}} f(\mathbf{R}), \end{aligned} \quad (13)$$

where $f(\mathbf{R})$ is the Fourier transform of $\ln E(\mathbf{k})$, and the sum is taken over all closed trajectories with odd windings in the y -direction (see Fig. 4a). The function $f(\mathbf{R})$ decays exponentially with distance, with the same correlation lengths ξ_n as the Majorana Green's functions (the correlation lengths determined by (6) and (7)). The physical interpretation of those exponents are the quasiclassical amplitudes of the vison tunneling around the torus[4]. The splitting (13) is dominated by the largest of the exponents, i.e., by the optimal trajectory (the choice of the optimal trajectory depends on the aspect ratio of the torus, and, because of the anisotropy, may not necessarily be the geometrically shortest one). This result

may formally be written as

$$\Delta \lesssim \exp \left(- \min_{\mathbf{R}} \operatorname{Re} \left[\frac{R}{\xi_{\mathbf{n}}} \right] \right), \quad (14)$$

where $\xi_{\mathbf{n}}$ is given by (6) and (7) [or, equivalently by (8)] with the vector \mathbf{n} in the direction of \mathbf{R} , and the minimization is performed over all displacements \mathbf{R} returning to the original point with an odd winding number in the y -direction (Fig. 4a).

Note that Eq. (14) neglects interference between different trajectories in Fig. 4a. Such an interference may additionally suppress the splitting, hence we put the \lesssim sign in (14). We can take the interference into account by performing not the full Fourier transformation in (13), but only the Fourier transformation in the y direction, leaving the k_x component of the wave vector quantized. We denote this quantization of k_x as $k_x \in \Lambda$, where Λ is the set of allowed values of k_x [necessarily real!] depending on L_x and on the boundary condition. Then repeating the above argument, we arrive at the estimate for the splitting:

$$\Delta \lesssim \exp \left(- \min \operatorname{Im} \mathbf{k} \mathbf{L}_y \Big|_{E(\mathbf{k})=0}^{k_x \in \Lambda} \right), \quad (15)$$

where the minimum is taken among positive values only. Because of the constraint $k_x \in \Lambda$, the expression (15) is invariant with respect to $\mathbf{L}_y \mapsto \mathbf{L}_y \pm \mathbf{L}_x$, as expected [any displacement \mathbf{R} in Fig. 4a with winding number one may be chosen as \mathbf{L}_y].

We have obtained the two estimates (14) and (15) both derived in the limit $L_y \gg 1$. One can verify that the estimate (14) is stronger than (15) when $L_x \gtrsim L_y \gg 1$, while (15) is stronger than (14) when $L_y \gg L_x \sim 1$ (quasi-one-dimensional limit). In the intermediate regime $L_y \gg L_x \gg 1$, both (14) and (15) reduce to the same result

$$\Delta \sim \exp \left(- \operatorname{Re} \left[\frac{L_y}{\xi_{\mathbf{n}}^*} \right] \right), \quad (16)$$

$$(\xi_{\mathbf{n}}^*)^{-1} = \min^{\operatorname{Re}} (-i \mathbf{n} \mathbf{k}) \Big|_{\operatorname{Im} \mathbf{L}_x \mathbf{k}=0}^{E(\mathbf{k})=0}.$$

Here \mathbf{n} is the vector perpendicular to \mathbf{L}_x and $L_y = \mathbf{n} \mathbf{L}_y$. The minimization is performed over the wave vector \mathbf{k} with its imaginary component parallel to \mathbf{n} . Thus defined correlation length $\xi_{\mathbf{n}}^*$ corresponds to the vison tunneling as a “wave front” (as a plane wave in the x direction) and is slightly different from $\xi_{\mathbf{n}}$ corresponding to the tunneling of a “point” vison, see Fig. 3 (this difference is due to the lattice anisotropy).

The splitting between Z_{++} and Z_{+-} translates into the exponentially small splitting between N_{eo} and N_{oo} given by the same expressions (14)–(16). Note that a vison tunneling in the y -direction relates the topological sectors with different parity of intersections with a contour running in the y -direction. Similar expressions apply for splitting in other pairs of topological sectors.

The splitting of the two topological sectors on a cylinder (or on a disc with one hole, which is topologically

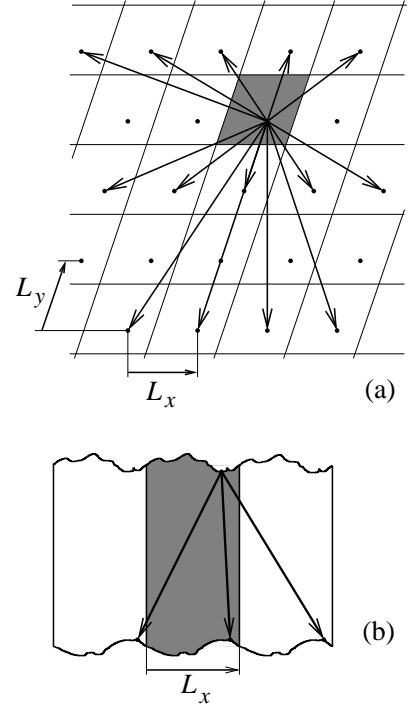


FIG. 4: The vison tunneling trajectories \mathbf{R} contributing to the splitting between partition functions on the torus and on the cylinder. **(a)** The torus is constructed by identifying points on the plane differing by multiples of the two basis vectors \mathbf{L}_x and \mathbf{L}_y . Equivalently, it may be described by identifying opposite sides of the unit cell (shaded parallelogram). The vectors \mathbf{R} contributing to the splitting between Z_{++} and Z_{+-} (or, equivalently, between N_{eo} and N_{oo}) [Eqs. (13) and (14)] belong to the lattice generated by \mathbf{L}_x and \mathbf{L}_y and have odd winding numbers in the y direction. **(b)** The tunneling trajectories \mathbf{R} determining the splitting between the topological sectors on the cylinder as given by Eq. (14). The cylinder is defined by identifying points differing by a multiple of \mathbf{L}_x .

equivalent to a cylinder) is derived in a way slightly different from our analysis of the torus. Consider a semi-infinite cylinder (or a plane with one hole of arbitrary size and shape). On such a system, we consider two different boundary conditions for Majorana fermions: periodic and antiperiodic as we go around the cylinder (around the hole, respectively). To those boundary conditions, there correspond the two matrices $A_{ij}^{(+)}$ and $A_{ij}^{(-)}$. Below we prove that one of those matrices has a zero eigenvalue (with the eigenvector localized near the boundary), and the other does not (in the general case).

The proof consists of four steps. First, we consider a semi-infinite cylinder of a particular geometry, with the straight boundary parallel to one of the lattice lines (Fig. 5a). For such a cylinder, the spectrum can be exactly computed, and the existence of the zero mode in one of the two topological sectors is easily verified (for this particular geometry, the zero mode is strictly localized at the boundary row of sites). Second, we note that the bulk

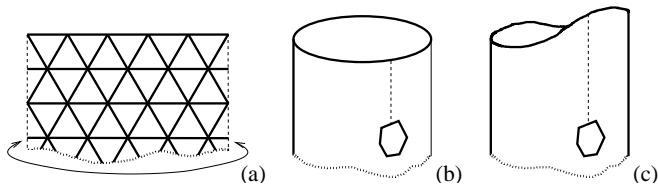


FIG. 5: **(a)** A particular geometry of the semi-infinite cylinder with the straight edge in the A direction. For this cylinder, the zero mode of the A_{ij} matrix (for one of the two boundary conditions) may be explicitly found. Arrows show identification of the two edges of the semi-infinite stripe. **(b)** The same cylinder as in (a), with a hole sufficiently far from the edge. Two different boundary conditions are possible across the dashed line. **(c)** A cylinder of arbitrary geometry with a hole far from the edge. Two different boundary conditions are possible across the dashed line.

spectrum of A_{ij} is gapped, and therefore there are only a finite number of states at small energies, and they are all localized near the boundaries. Since all eigenvalues of the antisymmetric matrix come in pairs $\pm iE$, the property of having a zero mode depends on whether there are even or odd number of subgap states. This parity can not be changed by any *local* deformation of the antisymmetric matrix A_{ij} and thus the zero mode (or its absence) is topologically stable (note that this argument resembles the proof of the topological stability of the zero mode in vortices in p -wave superconductors[24, 25]). Third, once the theorem proven for a particular geometry of the cylinder, we make a hole in this cylinder sufficiently far from the boundary (Fig. 5b). Then we can impose either periodic or antiperiodic boundary conditions across a line connecting the hole to the edge of the cylinder (dashed line in the figure). Switching the boundary conditions toggles on and off the zero mode at the cylinder edge. However, since the total parity of the subgap states (including both states at the cylinder edge and at the hole) is conserved, switching the boundary conditions across the dashed line also toggles the zero mode at the hole boundary. Thus we extend our theorem to the case of a hole in a plane (a sufficiently large cylinder may be regarded as a plane, from the point of view of states localized near the hole). Fourth, we repeat the previous argument for a cylinder of arbitrary geometry with a hole in it (Fig. 5c), and thus establish the presence of the zero mode at the cylinder edge for one of the two boundary conditions. This completes the proof.

It is the zero modes which determine the splitting between the topological sectors on a cylinder. The partition functions of the Majorana fermions on the cylinder with periodic and antiperiodic boundary conditions are

$$Z_+ = N_e + N_o, \quad Z_- = N_e - N_o \quad (17)$$

(or vice versa, depending on the choice of the gauge for A_{ij}), where N_e and N_o are the numbers of dimer coverings in the even and odd sectors. The splitting between N_e and N_o is given by $\Delta = Z_-/Z_+$ and is determined

by the splitting of the two zero modes (contributing to Z_-). This splitting is in turn determined by the exponential tails of the zero modes away from the boundary: the exponential dependence of the splitting on the cylinder length has the same correlation length as the decay of the zero modes. Similarly to the case of the torus, this exponential decay may be estimated in two ways. In the first approach, the zero mode is constructed as a linear combination of Green's functions localized near the boundary. Explicitly, we consider the zero mode Ψ_0 on the “unfolded” cylinder (Fig. 4b) and act on it with the matrix A_{ij} defined *on the whole plane*. The resulting wavefunction contains positions and amplitudes of the sources for the Green's functions to reproduce the original zero mode Ψ_0 . This representation proves that the decay of zero modes (and hence the splitting Δ) obeys the estimate (14) with the minimization performed over all possible vectors \mathbf{R} connecting the opposite edges of

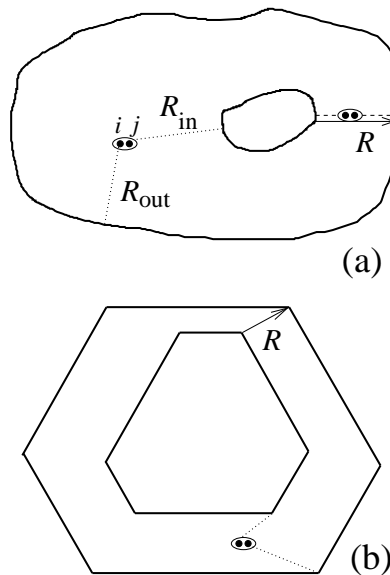


FIG. 6: The vison tunneling trajectories determining the splitting between the topological sectors in the plane geometry (a disc with a hole). **(a)** In the general situation, the splitting is determined by Eq. (14) with the minimization over trajectories \mathbf{R} connecting the hole to the external boundary. The splitting of the local dimer correlation functions (20) is determined by the two tunneling events: vison tunneling from the inner boundary to the location of the involved dimers (R_{in}) and then further to the outer boundary (R_{out}). The two possible situations are shown: the splitting near the optimal tunneling trajectory have the same exponential dependence as the direct tunneling from the inner to the outer boundary (dashed line), while at locations far from the optimal tunneling trajectory, the splitting is smaller (dotted line). **(b)** In the special case of polygon boundaries with their segments parallel to lattice directions (A directions), only trajectories connecting corners of the boundaries should be taken into account in (14) and (20), since vison tunneling from the boundaries is suppressed.

the cylinder (Fig. 4b) [see also the analogous discussion below of the zero modes in the plane geometry]. Alternatively, we may represent the zero mode as a linear combination of plane waves quantized in the x -direction and decaying in the y direction, which leads to Eq. (15). The relation between those two estimates is the same as for the case of the torus, with the same expression (16) valid in the regime $L_x \gg L_y \gg 1$.

We need to remark, however, that in the case of the cylinder, the formulas (14)–(16) do not properly take into account interference of tunneling trajectories starting or ending at *neighboring* points of the boundary. As a consequence, the expressions (14)–(16) give good (most likely exact) asymptotic estimates in the case of ragged boundaries, but may strongly overestimate splitting in the case of a regular edge. For example, at the straight edge shown in Fig. 4b, the zero mode is exactly localized at the boundary layer of sites, and therefore the splitting of the topological sectors on a cylinder with such an edge is *exactly zero*, in contrast with (14)–(16).

Our discussion of the cylinder may be directly extended to the plane geometry (holes in the disc), with the only difference that there are no counterparts of Eqs. (15) and (16) in this case. Consider specifically the simplest possible geometry: a disc with a hole in it (Fig. 6a). A reference line defining the two topological sectors is drawn to connect the two boundaries (the external boundary and the hole boundary). Similarly to the cylindrical geometry, the splitting of the partition functions Z_e and Z_o is given by the splitting of the zero modes at the two boundaries. Our proof of the existence of zero modes may be easily extended to show that in the plane geometry, the hole encircling an *odd* number of sites hosts a zero mode for the *periodic* boundary conditions around the hole, while a hole with an *even* number of internal sites has a zero mode for the *anti-periodic* (vison-like, see the last section of the paper) boundary conditions. For a hole with an *odd* number of internal sites, the zero mode may be constructed as a linear combination of Green's functions with sources located near the boundary (the proof of this statement is similar to that in the cylindrical geometry: it follows from acting on the zero mode with the operator A_{ij} defined on the whole plane including the hole interior). Therefore the zero mode decays with the same correlation lengths ξ_n as the Majorana Green's function. The same result may also be proven for a hole with an *even* number of internal sites: the proof is a straightforward generalization of the theorem about the correlation length of the vison operator proven in the last section of the paper. Thus, for any type of hole, the splitting between Z_e and Z_o is given by Eq. (14), with the minimization performed over all trajectories \mathbf{R} connecting the inner and the outer boundaries (Fig. 6a).

Note however that for certain special geometries — in particular, those involving straight edges stretching along the A directions (along the lattice lines, Fig. 5) — Eq. (14) may overestimate the splitting. An analysis of

the specific case of plane geometries with only straight edges along the A directions reveals that tunneling of visons from the straight edges is suppressed (see also a similar remark about the zero modes at straight edges of cylinders), and that the splitting is given by Eq. (14) with the tunneling trajectories R drawn between *corners* of the boundaries (Fig. 6b).

IV. LOCAL DIMER CORRELATIONS AND GROUND-STATE ENERGY SPLITTING UNDER PERTURBATION

Our discussion of the splitting in the partition functions may be extended to compute the exponentially small splitting in correlation functions of local operators. Consider first the simplest correlation function — the average dimer density on a given link $\langle n_{ij} \rangle$ on a cylinder or on a disc with a hole. In the $+/-$ sectors, this expectation value may be found as the Majorana Green's function $G_{ij} = \langle a_i a_j \rangle$. The partition functions and the Green's functions with periodic/antiperiodic boundary conditions will be denoted as Z_+ , Z_- , and as G_{ij}^+ , G_{ij}^- , respectively. As explained in the previous section, with one of those boundary conditions, the matrix A_{ij} has zero modes at the two boundaries. Without loss of generality, we assume that the zero modes appear in the “ $-$ ” sector. If we consider only one boundary (a semi-infinite cylinder or only one hole), the zero mode at this boundary may be chosen to be real. We denote such zero modes by $\Psi_a(i)$ and $\Psi_b(i)$ (a and b label the two boundaries near which the zero modes are localized). In a finite system, these two wave functions are hybridized and split. The two conjugate wave functions $\Psi_1 = \Psi_a + i\Psi_b$ and $\Psi_2 = \Psi_a - i\Psi_b$ have small non-zero eigenvalues $\pm iE_0$ [the value of E_0 is exponentially small in system size and obeys the estimates (14)–(16)]. The difference between the expectation values of n_{ij} in the *odd* and *even* sectors is

$$\begin{aligned} \langle n_{ij} \rangle_o - \langle n_{ij} \rangle_e &= \frac{Z_+ G_{ij}^+ - Z_- G_{ij}^-}{Z_+ - Z_-} - \frac{Z_+ G_{ij}^+ + Z_- G_{ij}^-}{Z_+ + Z_-} \\ &= \frac{2Z_+ Z_-}{Z_+^2 - Z_-^2} (G_{ij}^+ - G_{ij}^-) \approx \frac{2Z_-}{Z_+} (G_{ij}^+ - G_{ij}^-) \end{aligned} \quad (18)$$

(in the last equality we have used $Z_- \ll Z_+$).

Further, the Green's functions may be rewritten as sums over eigenvectors $G_{ij} = \sum_n \Psi_n(i) \Psi_n^*(j) / iE_n$. The main contribution to $G_{ij}^+ - G_{ij}^-$ comes from the zero modes Ψ_1 and Ψ_2 in G_{ij}^- . The exponentially small prefactor Z_-/Z_+ is canceled by the exponentially small denominator E_0 in G_{ij}^- , and to the exponential precision we find

$$\langle n_{ij} \rangle_o - \langle n_{ij} \rangle_e \sim \Psi_a(i) \Psi_b(j) - \Psi_b(i) \Psi_a(j) \quad (19)$$

Graphically, this result may be depicted as the sum of the two diagrams in Fig. 7a.

This diagrammatic approach may be extended to the even-odd splitting in higher-order correlation functions.

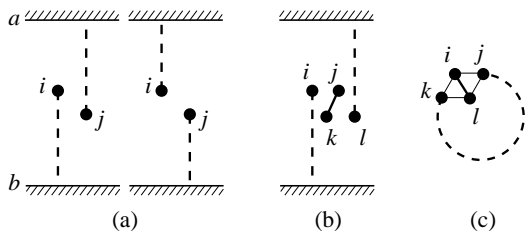


FIG. 7: Diagrams involved in splitting between correlation functions in different topological sectors. **(a)** The two diagrams contributing to the splitting of the average dimer density $\langle n_{ij} \rangle$ between the odd and even sectors on the cylinder. The two edges of the cylinder are labeled a and b . The dashed lines represent the zero-mode wave functions Ψ_a and Ψ_b . **(b)** One of the diagrams contributing to the splitting of the four-point correlation function $\langle n_{ij} n_{kl} \rangle$ on the cylinder. The dashed lines represent the zero-mode wave functions Ψ_a and Ψ_b ; the solid line denotes the bulk Green's function G_{jk} . **(c)** One of the diagrams contributing to the splitting of the four-point correlation function $\langle n_{ij} n_{kl} \rangle$ on the torus. The thick solid line denotes the bulk Green's function G_{il} . The dashed line denotes the Green's function with a winding around the torus $G_{j,k+\mathbf{R}}$, where the winding vector \mathbf{R} is one of those shown in Fig. 4.

The diagrams are drawn by pairing all Majorana fermions in the correlation function (4) according to the Wick rule, except for one pair which is connected to the boundaries. To “internal” couplings, we associate the bulk Green's functions, while for the “external” lines, we associate the zero-mode wave functions as in (19) (an example of such a diagram is shown in Fig. 7b).

Furthermore, the same type of diagrammatic rules may be derived for the case of torus, with the only difference that the “external line” must in this case be closed and associated with the Green's function $G_{i,j+\mathbf{R}}$, where the vector \mathbf{R} winds around the torus with the appropriate winding number (as in Fig. 4a). An example of such a diagram is shown in Fig. 7c.

In the case of cylindrical and plane geometry, the smallness of the correlation-function splitting follows from the exponential behavior of the boundary zero modes. Since the zero modes rapidly decay away from the boundaries, the splitting (19) is exponentially small in the system size (at least as small as the estimates (14)–(16) or even smaller). The expression for the splitting may be written as

$$\langle n_{ij} \rangle_o - \langle n_{ij} \rangle_e \sim \exp \left[-\frac{R_{\text{in}}}{\xi_{\text{in}}} - \frac{R_{\text{out}}}{\xi_{\text{out}}} \right], \quad (20)$$

where R_{in} and R_{out} are the optimal tunneling trajectories from the link (ij) to the inner and outer boundaries, and ξ_{in} and ξ_{out} are the corresponding correlation lengths (Fig. 6a). If the system has a “weak spot” — a preferred vison tunneling trajectory, the correlations in the immediate vicinity of that trajectory are most sensitive to the choice of the topological sector. Correlations away from the optimal trajectory have a weaker splitting between

the sectors. On the torus, there is no “optimal tunneling trajectory” because of the translational symmetry, and the correlation-function splitting is given by (14)–(16), independently of the position of the involved operator.

The above results allow us to estimate the energy splitting in the perturbed Rokhsar–Kivelson model to the first order of the perturbation theory. Physically, two types of perturbations may be of interest. First, we consider the case $v/t < 1$ in the Hamiltonian (1), in which case the ground-state energy is no longer zero. The ground-state energy may be estimated to the linear order in $(1-v/t)$ as $(v-t)\langle H_v \rangle_{RK}$, where H_v is the potential (proportional to v) term in the Hamiltonian (1), and the average is taken in the unperturbed system. H_v is a four-point (dimer-dimer) correlation function, and from our previous discussion it follows that the splitting of $\langle H_v \rangle_{RK}$ in different topological sectors is exponentially small in the system size with the exponent estimated by (14)–(16). Second, similar exponential smallness may also be derived for the energy splitting under the influence of disorder (again, to the linear order in the disorder potential). Note that the energy splitting is more sensitive to disorder in the vicinity of the optimal vison tunneling trajectory.

Within our method, the exponentially small response of the energy splitting to the perturbation can be derived only to the lowest order of the perturbation theory. Extending those results to higher orders requires information on the excited states at the RK point. This goes beyond the scope of this paper, since the excited states are not accessible by the Pfaffian technique.

V. VISON OPERATORS AND CORRELATIONS

The concept of a vison can be made more transparent by introducing a “vison operator”. Given two elementary plaquettes (triangles) of the lattice and a contour Γ connecting them, we can define the product of two vison operators $V_1 V_2$ as

$$V_1 V_2 = (-1)^{N_\Gamma} = \prod_{\Gamma} (1 - 2n_{ij}), \quad (21)$$

where N_Γ is the number of dimers intersecting the contour Γ , and the last product is taken over all links (ij) intersecting Γ (Fig. 8) [14]. It can be easily seen that deforming the contour Γ while keeping the end points fixed may only change the sign of this operator (depending on whether between the old and the new contour lies odd or even number of sites). This allows us to define a single vison operator (up to a sign; more precisely, the vison operator is defined on the frustrated dual lattice, with reversing its sign when moved around one site of the original lattice). For a single vison operator, the contour Γ is drawn either to infinity (for an infinite system) or to the boundary. In a finite system without boundaries (e.g. torus), vison operators may appear only in pairs.

In the Majorana fermion technique (2), the vison operator is equivalent to changing the boundary conditions

(from periodic to anti-periodic and vice versa, i.e., placing a Z_2 twist) across the contour Γ . Thus switching topological sectors on a cylinder as described above is equivalent to placing a pair of visons in the cylinder openings. On a torus, switching topological sectors is achieved by creating a vison-vison pair, subsequently moving one of the two visons around the torus and annihilating it back with the other vison.

Applying a vison operator as defined above to the ground state does not produce an eigenstate of the Hamiltonian (1). However, preliminary studies show that the state thus obtained is close to the actual low-lying excitations[20]. A localized excitation (a wavepacket) may be classified as either vison-like or non-vison-like depending on whether it originates a cut Γ across which the boundary conditions are changed. Based on the available numerical studies [20], we believe that the lowest excitations belong to the vison-like sector; this also conforms to the existing field-theoretical description of the RVB liquid [4] (studies of related models with an exact construction of the vison excitations appeared recently in Refs. 9, 10). We expect that the leading exponential asymptotics of long-distance correlators of vison-like operators is dominated by the topological effect of changing the boundary conditions across the cut Γ , and only finite prefactors depend on the details of the involved operators. In other words, the correlation length of vison-like operators is universal and may be determined, for example, from the pairwise correlation function $\langle V_1 V_2 \rangle$ as defined in (21).

We can prove that the vison correlation length equals that for Majorana fermions. For the same reason as for a hole in the plane (see discussion above), a vison on an infinite plane produces a zero mode of the matrix A_{ij} . Thus the vison correlation length is determined by the decay of this zero mode at large distances. The matrix A_{ij} in the presence of the vison may be written as $A_{ij} = A_{ij}^{(0)} + \delta A_{ij}$, where $A_{ij}^{(0)}$ is the matrix of hopping amplitudes without the vison and δA_{ij} is localized at the cut drawn from the vison. Note that the zero mode does not depend on the trajectory of the cut (up to a gauge transformation). The equation on the zero mode $(A^{(0)} + \delta A)\Psi_0 = 0$ may be

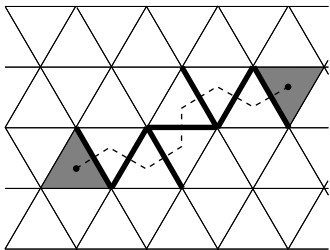


FIG. 8: The product of the two vison operators. The visons are placed in the shaded triangles. The contour Γ connecting them is shown as the dashed line. The bold links are those involved in the operator (21).

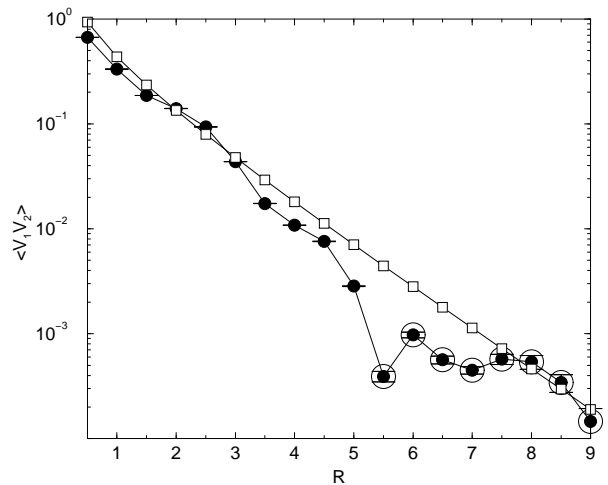


FIG. 9: The variational Monte Carlo results of the vison-vison correlation function (21) in the A direction. The plot is in the linear-logarithmic scale, with the distance measured in the lattice spacings. The solid dots are the numerical results (the circles around dots indicate negative values). The magnitude of the numerical data should be compared to the analytic expression $R^{-1/2} \exp(-\text{Re } R/\xi_A)$ (empty squares), where ξ_A is given by (9). The calculation was performed on the 50×50 torus with averaging over 10^6 dimer configurations (error bars are shown).

rewritten as $\Psi_0 = -[A^{(0)}]^{-1} \delta A \Psi_0$. From this expression, it follows that the exponential decay of Ψ_0 away from the vison has the asymptotics of $[A^{(0)}]^{-1}$ which is exactly the Green's functions of Majorana fermions (5). This finishes the proof. Note that this result is consistent with our findings for the splitting between topological sectors and with their interpretation in terms of vison tunneling amplitudes. Furthermore, our result about the decay of the zero mode at the point-like vison is a particular case of a more general statement about the zero modes at even-size holes (see our discussion in Section III): the point-like vison may be considered as a hole of size zero; the proof may be extended in a straightforward way to cover the general case of an even-size hole.

To illustrate our result on the equality between the correlation lengths for visons and for Majorana fermions, we have calculated numerically the vison-vison correlation function in the A direction. The calculation was performed by the variational Monte Carlo method: the vison correlation function was computed as the average over a suitable random walk in the space of all dimer configurations[7]. Figure 9 shows the numerical results of the calculation (for distances up to 9 lattice spacings, on the lattice of 50×50 torus), together with the analytic expression $R^{-1/2} \exp(-\text{Re } R/\xi_A)$. We have no analytic expression for the phase of the oscillating part of the correlation function (arising from the imaginary part of ξ_A^{-1}) and therefore compare only the overall magnitude of the correlation function. The agreement in the magnitude

and the change of sign in the vison correlator (a signature of the oscillatory behavior) are consistent with our analytical prediction of the correlation length (9).

To summarize, we have shown that in the dimer model (1) on the triangular lattice, at the RK point $t = v$, both dimer and vison correlations decay exponentially with the distance. Dimer correlations may be expressed as finite products of the Green's functions of auxiliary Majorana fermions for which the correlation length is computed explicitly. We have further shown that the vison correlation length coincides with that of Majorana fermions. The same correlation length also governs the splitting between correlation functions in different topological sectors (14)–(16). Thus the Rokhsar–Kivelson dimer model provides an example of the system where

the topological ground-state properties of the RVB liquid may be explicitly verified.

We thank L. Ioffe, G. Blatter, T. Senthil, and O. Motrunich for useful discussions. Support from the program “Quantum Macrophysics” of Russian Academy of Sciences, the program “Physics of Quantum Computations” of Russian Ministry of Science, SCOPES program of Switzerland, Dutch Organization for Fundamental research (NWO), RFBR grant 01-02-17759, and the Swiss National Foundation is gratefully acknowledged.

P. S. At the final stage of the manuscript preparation, we have learned about the recent work [26], where the same dimer model is studied. Many of our results in Section II overlap with those derived in that work. Among other results, Ref. 26 also contains a more detailed analysis of the Majorana Green's functions.

-
- [1] P. W. Anderson, *Science* **235**, 1196 (1987).
 - [2] S. A. Kivelson, D. S. Rokhsar, and J. P. Sethna, *Phys. Rev. B* **35**, 8865 (1987).
 - [3] E. Fradkin and S. Kivelson, *Mod. Phys. Lett. B* **4**, 225 (1990).
 - [4] T. Senthil and M. P. A. Fisher, *Phys. Rev. B* **62**, 7850 (2000); *ibid.* **63**, 134521 (2001).
 - [5] G. Misguich et al, *Phys. Rev. B* **60**, 1064 (1999); R. Sindzingre, C. Lhuillier, and J.-B. Fouet, *cond-mat/0110283*; G. Misguich et al, *cond-mat/0112360*.
 - [6] R. Moessner and S. L. Sondhi, *Phys. Rev. Lett.* **86**, 1881 (2001).
 - [7] L. Balents, M. P. A. Fisher, and S. M. Girvin, *cond-mat/0110005*.
 - [8] T. Senthil and O. Motrunich, *cond-mat/0201320*; O. Motrunich and T. Senthil, *cond-mat/0205170*.
 - [9] G. Misguich, D. Serban, V. Pasquier, *cond-mat/0204428*.
 - [10] L. B. Ioffe and M. V. Feigelman, *cond-mat/0205186*.
 - [11] R. Moessner, S. L. Sondhi, and E. Fradkin, *cond-mat/0103396*.
 - [12] N. Read and S. Sachdev, *Nucl. Phys. B* **316**, 609 (1989).
 - [13] S. Liang, B. Doucot, and P. W. Anderson, *Phys. Rev. Lett.* **61**, 365 (1988); B. Sutherland, *Phys. Rev. B* **37**, 3786 (1988).
 - [14] N. Read and B. Chakraborty, *Phys. Rev. B* **40**, 7133 (1989).
 - [15] D. S. Rokhsar and S. A. Kivelson, *Phys. Rev. Lett.* **61**, 2376 (1988).
 - [16] N. Bonesteel, *Phys. Rev. B* **40**, 8954 (1989).
 - [17] L. S. Levitov, *Phys. Rev. Lett.* **64**, 92 (1990).
 - [18] L. B. Ioffe et al, *Nature* **415**, 503 (2002).
 - [19] P. W. Kasteleyn, *J. Math. Phys.* **4**, 287 (1963); S. Samuel, *J. Math. Phys.* **21**, 2806 (1980).
 - [20] L. B. Ioffe, unpublished.
 - [21] M. E. Fisher and J. Stephenson, *Phys. Rev.* **132**, 1411 (1963).
 - [22] D. A. Ivanov and T. Senthil, *cond-mat/0204043*.
 - [23] T. Regge and R. Zecchina, *J. Phys. A* **33**, 741 (2000) [*cond-mat/9909168*]; R. Zecchina, *Physica A*, **302**, 100 (2001).
 - [24] N. Read and D. Green, *Phys. Rev. B* **61**, 10267 (2000).
 - [25] D. A. Ivanov, *Phys. Rev. Lett.* **86**, 268 (2001).
 - [26] P. Fendley, R. Moessner, and S. L. Sondhi, *cond-mat/0206159*.